Theoretical exploration of phase transitions in a cavity-BEC system with two crossed optical pumps

Wei Qin,* Dong-Chen Zheng,* Zhao-Di Wu, Yuan-Hong Chen, and Renyuan Liao†

Fujian Provincial Key Laboratory for Quantum Manipulation and New Energy Materials, College of Physics and Energy, Fujian Normal University, Fuzhou 350117, China

and Fujian Provincial Collaborative Innovation Center for Advanced High-Field Superconducting Materials and Engineering, Fuzhou 350117, China

(Received 23 October 2023; accepted 20 December 2023; published 8 January 2024)

We consider a Bose-Einstein condensate inside an optical cavity and two crossed coherent pump fields. We determine perturbatively the phase boundary separating the normal superfluid phase and the superradiance phase. In the regime of negative cavity detuning, we map out the phase diagrams for both an attractive and a repulsive optical lattice. It turns out that the situation is quite different in the two cases. Specifically, in the case of an attractive lattice, if a system is in the superradiant phase with one pump laser, adding another pump does not drive the system out of the superradiance phase, while for the repulsive lattice, increasing another pump potential has suppressive effects on the superradiance. We also find that, in the case of an attractive lattice, equally increasing two pump lattice potentials can induce a transition from the normal phase to the superradiance phase. In stark contrast, for the repulsive lattice, the system will remain in the normal phase as the pump depths are tuned within a wide range, independently of the cavity detuning and the decay rate.

DOI: 10.1103/PhysRevA.109.013310

I. INTRODUCTION

Loading ultracold quantum gases into single or multiple high-finesse cavities provides a versatile platform to explore many-body phenomena [1–11]. The coupling between the degenerate quantum gases and quantized radiation fields in cavities gives rise to controllable long-range interactions, which is dominant in many-body phases [12,13]. Transversely driving a Bose-Einstein condensate (BEC) inside an optical cavity is a typical example, which allows us to achieve the Dicke model and a self-organization phase [12,14–21]. Taking the atoms' spins into account, one single cavity can also mediate spin-dependent interactions, realize single-mode Dicke spin models [22–25], and simulate a nondegenerate two-mode Dicke model [26,27]. With two crossed linear cavities, it is possible to demonstrate the coupling between two order parameters [28–30], realize different supersolid formation, and even engineer a continuous U(1) symmetry in real space and cavity space [31–34] so that Higgs and Goldstone modes can be monitored and manipulated [35].

Scattering photons into cavities, companied with the self-organization of quantum gases, lies at the heart of these phenomena, which is also referred to as superradiance. Usually, an attractive potential, rather than a repulsive one, is expected to induce superradiance since, intuitively, the buildup of any additional repulsive potential seems to cost energy and hence prohibits self-organization. Actually, most experiments implement a red-detuned pump laser to drive atoms so that an attractive standing-wave lattice can be generated. However, a repulsive pump potential, generated by a blue-detuned optical pump, is also able to produce superradiance, which has been verified theoretically and experimentally [36–40].

In practice, such a cavity-BEC system is commonly driven by a single-pump laser. It is hard to resist the temptation to ask what if there is more than just one pump as well as what the situation is in the case of an attractive or a repulsive optical lattice. It is not a trivial question to answer since additional pumps produce a two-dimensional periodic potential and lower the symmetry of the system compared with the case of one pump. In this work we address this question by considering a cavity-BEC system in the presence of two crossed optical pumps and we also take the interference between the two pumps into account. By mapping out the phase diagrams, we conclude that adding another pump will increase the tendency of a transition towards superradiance in the case of an attractive lattice and suppress the tendency in the case of a repulsive lattice. We also find that the repulsive rectangular lattice (equal pump lattice depths) cannot induce superradiance within a wide range of pump depths, which is independent of the cavity detuning and decay rate.

II. MODEL AND FORMALISM

In Fig. 1 we consider a BEC (orange) inside a high-finesse optical Fabry-Pérot resonator exposed to a cavity laser beam (yellow) and two pump laser beams (green and blue). The angle between the cavity beam and per pump beam is 60°, as shown in Fig. 1(a). We focus on the two-dimensional case, where the atoms' motion along $\hat{z}$ can be frozen by tight confinement and bosons can only move in the xy plane [41].

The decay rate of the cavity field is κ. Within the dipole and rotating-wave approximation, the effective many-body Hamiltonian in a frame rotating at the pump laser frequency [1,27] is given by

$$\hat{H} = \int d\mathbf{r}\, \hat{\Psi}^\dagger(\mathbf{r})\left(\frac{\hat{\mathbf{p}}^2}{2m} + \frac{\hbar}{\Delta_a}\hat{E}^\dagger\hat{E}\right)\hat{\Psi}(\mathbf{r}) - \hbar\Delta_c\hat{a}^\dagger\hat{a}, \quad (1a)$$

$$\hat{E} = \sum_{i=1,2}\Omega_i\cos(\mathbf{k}_i\cdot\mathbf{r}) + g\cos(\mathbf{k}_c\cdot\mathbf{r}+\phi)\hat{a}, \quad (1b)$$

*These authors contributed equally to this work.
†ryliao@fjnu.edu.cn

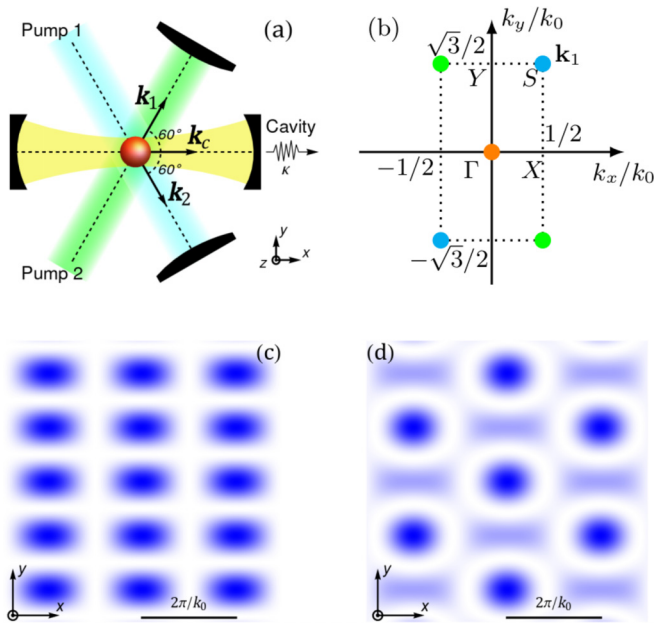

FIG. 1. (a) Schematic of the experimental setup. A BEC (orange) inside a high-finesse optical resonator is exposed to pump laser beam 1 (green) and pump laser beam 2 (blue). Photons scattered by the atoms populate the cavity mode (yellow), with coherent field amplitude α that can be detected when leaking from the cavity. The angles between the cavity beam and per pump beam are both 60°. (b) Wave-vector (momentum) distributions of the BEC. The orange point marks the condensed state in the absence of photons scattering into the cavity, while green (blue) points are the steady states of condensation scattered by pump 1 (2) in superradiant phase. The dotted line is the boundary of the first Brillouin zone for the two-dimensional rectangular lattice of the combined pump fields. Calculated density modulations for equal pump lattice depths are shown (c) without and (d) with the intracavity field, respectively, for red atomic detuning $\Delta_a < 0$. In the case of $\Delta_a > 0$, there is no superradiant phase under equal pump depths within red atomic detuning $\Delta_c < 0$, but the density pattern is the same as in (c) in the absence of the intracavity field.

where $\hat{\Psi}^\dagger$ ($\hat{\Psi}$) is the creation (annihilation) operator for bosonic atoms with mass m and momentum $\hat{\mathbf{p}} = -i\hbar\nabla$ and $\hat{a}^\dagger$ ($\hat{a}$) is the photon creation (annihilation) operator for the cavity mode. Here we consider pump beams that have the same frequency ω_p, which is far detuned by $\Delta_a = \omega_p - \omega_a$ from the atomic resonance at frequency ω_a. The cavity frequency ω_c is closely detuned by $\Delta_c = \omega_p - \omega_c$ from the pump frequency, and we stay within only $\Delta_c < 0$ throughout this work. Here Ω_j ($j = 1, 2$) are the Rabi frequencies for pump beams and g is single-photon Rabi frequency of the cavity mode. The wave vectors of the pump beams and cavity light are given by $\mathbf{k}_j = k_0\cos(60^\circ)\hat{x} + (-1)^{j+1}k_0\sin(60^\circ)\hat{y}$ and $\mathbf{k}_c = k_0\hat{x}$, respectively, as shown in Fig. 1(a). Here k_0 is the wave-vector magnitude of the pumping lasers and the cavity mode. We choose recoil energy $E_R = \hbar^2k_0^2/2m$ as the energy unit and set $\hbar = 1$ for simplicity. The relative spatial phase between the pumps and cavity field is denoted by ϕ, which can be adjusted experimentally [31,42], and is assumed to be in phase at the origin, namely, $\phi = 0$.

At the zero-temperature limit, all atoms occupy the lowest-energy Bloch state $|\Psi^{(1)}(0)\rangle$ in the absence of intracavity photons, where $|\Psi^{(j)}(\mathbf{k})\rangle$ denotes the jth band eigenstates of the single-particle Hamiltonian

$$\hat{\mathcal{H}}_0 = \frac{\hat{\mathbf{p}}^2}{2m} + \mathrm{sgn}(\Delta_a)[V_1\cos^2(\mathbf{k}_1\cdot\mathbf{r}) + V_2\cos^2(\mathbf{k}_2\cdot\mathbf{r}) + 2\sqrt{V_1V_2}\cos(\mathbf{k}_1\cdot\mathbf{r})\cos(\mathbf{k}_2\cdot\mathbf{r})]. \quad (2)$$

Here we define pump lattice depths $V_i = \Omega_i^2/|\Delta_a|$ ($i = 1, 2$) and $\mathrm{sgn}(\Delta_a)$ gives the sign of atomic detuning Δ_a. Indeed, $\mathrm{sgn}(\Delta_a)$ determines whether the effective pump potential is attractive (negative) or repulsive (positive).

Intracavity photons are scattered by atoms from the transverse pump lasers into the cavity mode and vice versa. It is sufficient to consider the two-photon scattering processes through the phase transition. Equivalently, starting from the lowest-energy Bloch state $|\Psi^{(1)}(0)\rangle$ of the BEC, only $|\Psi^{(j)}(\mathbf{k}_1)\rangle$ can be reached by applying the scattering operator

$$\hat{\Theta} = \sum_{i=1,2}\sqrt{V_i}\cos(\mathbf{k}_i\cdot\mathbf{r})\cos(\mathbf{k}_c\cdot\mathbf{r}). \quad (3)$$

Hence the atomic field operator can be expanded as

$$\hat{\Psi}(\mathbf{r}) \approx \langle\mathbf{r}|\Psi^{(1)}(0)\rangle\hat{b}_0 + \sum_j\langle\mathbf{r}|\Psi^{(j)}(\mathbf{k}_1)\rangle\hat{b}_j, \quad (4)$$

where $\hat{b}_0$ and $\hat{b}_j$ are bosonic annihilation operators for states $|\Psi^{(1)}(0)\rangle$ and $|\Psi^{(j)}(\mathbf{k}_1)\rangle$, respectively. The sums are over all band indices $j = 1, 2, \ldots$, while the particle number conservation $\hat{b}_0^\dagger\hat{b}_0 + \sum_j\hat{b}_j^\dagger\hat{b}_j = N$ should be satisfied, with N the total atom number. Substituting Eq. (4) into Eq. (1) yields the effective Hamiltonian

$$\hat{H}_{\mathrm{eff}} = -\tilde{\Delta}_c\hat{a}^\dagger\hat{a} + \sum_j(E_j - E_0)\hat{b}_j^\dagger\hat{b}_j + (\hat{a}^\dagger + \hat{a})\sum_j(\nu_j\hat{b}_j^\dagger\hat{b}_0 + \mathrm{H.c.}), \quad (5)$$

where the effective cavity detuning is defined as $\tilde{\Delta}_c = \Delta_c - \mathrm{sgn}(\Delta_a)U_0N\langle\Psi^{(1)}(0)|\cos^2(\mathbf{k}_c\cdot\mathbf{r})|\Psi^{(1)}(0)\rangle$, and here we set $U_0 = g^2/|\Delta_a|$. The scattering matrix elements are given by $\nu_j = \mathrm{sgn}(\Delta_a)\sqrt{U_0}\theta_j$, with $\theta_j = \langle\Psi^{(j)}(\mathbf{k}_1)|\hat{\Theta}|\Psi^{(1)}(0)\rangle$. In addition, E_0 and E_j are eigenvalues of $\hat{\mathcal{H}}_0$ corresponding to $|\Psi^{(1)}(0)\rangle$ and $|\Psi^{(j)}(\mathbf{k}_1)\rangle$, respectively.

We proceed with mean-field description by taking the average values $\langle\hat{a}\rangle = \alpha$, $\langle\hat{b}_0\rangle = \psi_0$, and $\langle\hat{b}_j\rangle = \psi_j$. The atomic fields are governed by the Heisenberg equation $i\partial_t\hat{b}_j = [\hat{b}_j, \hat{H}_{\mathrm{eff}}]$. We seek a steady state in which $\partial_t\psi_j = 0$, gaining $\psi_j = (\alpha^* + \alpha)\nu_j\psi_0/(E_0 - E_j)$. Together with the normalization condition $|\psi_0|^2 = N - \sum_j|\psi_j|^2$, we retain the ground-state energy up to the fourth order in the amplitude of α,

$$\mathcal{E}_\alpha \approx -\tilde{\Delta}_c\alpha^*\alpha - NU_0\chi(\alpha^* + \alpha)^2 + NU_0^2\chi\eta(\alpha^* + \alpha)^4. \quad (6)$$

Here we define the susceptibility $\chi = \sum_j|\theta_j|^2/(E_j - E_0)$ and $\eta = \sum_j|\theta_j|^2/(E_j - E_0)^2$. Note that χ and η are functions of V_1 and V_2 and they also depend on $\mathrm{sgn}(\Delta_a)$. Meanwhile, the Heisenberg equation of the photon operator is given by $i\partial_t\hat{a} = [\hat{a}, \hat{H}_{\mathrm{eff}}] - i\kappa\hat{a}$. The steady condition $\partial_t\alpha = 0$ leads to $\alpha = \mathrm{sgn}(\Delta_a)\sqrt{U_0}\Theta/(\tilde{\Delta}_c + i\kappa)$, where an order parameter $\Theta = \int d\mathbf{r}\langle\hat{\Psi}^\dagger\hat{\Theta}\hat{\Psi}\rangle$ is introduced, so the energy can be

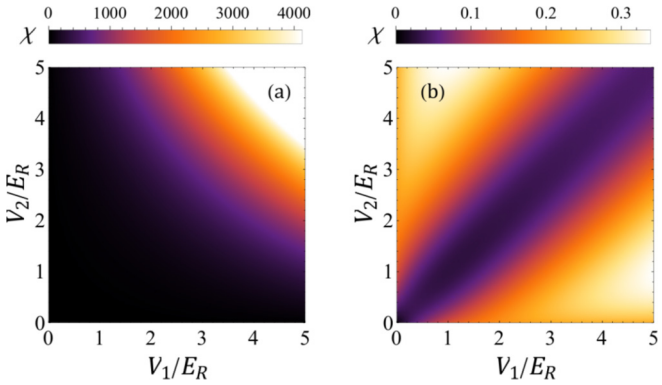

FIG. 2. Dimensionless susceptibility χ as a function of V_1/E_R and V_2/E_R for (a) $\Delta_a < 0$ and (b) $\Delta_a > 0$. The brightness of the region is proportional to the magnitude of χ: A brighter region represents a larger χ.

transformed into

$$\mathcal{E}_\Theta \approx -\frac{\tilde{\Delta}_c U_0}{\tilde{\Delta}_c^2+\kappa^2}\left(1+\frac{4\tilde{\Delta}_c N U_0 \chi}{\tilde{\Delta}_c^2+\kappa^2}\right)\Theta^2+\frac{16\tilde{\Delta}_c^4 N U_0^4 \chi \eta}{\left(\tilde{\Delta}_c^2+\kappa^2\right)^4}\Theta^4. \tag{7}$$

The coefficient of the fourth-order term being positive guarantees the stability of the system. We minimize the ground-state energy (7) with respect to the order parameter Θ, yielding the established superradiant phase condition

$$-\frac{4\tilde{\Delta}_c N U_0}{\tilde{\Delta}_c^2+\kappa^2}\chi > 1. \tag{8}$$

Note that we deal with only $\tilde{\Delta}_c < 0$ here. In the normal phase, we have $\Theta = 0$ as expected, while in superradiance the system has one of the two solutions

$$\Theta = \pm\frac{N\eta\chi(\tilde{\Delta}^2+\kappa^2)\sqrt{\tilde{\Delta}^2+\kappa^2+4NU_0\tilde{\Delta}_c\chi}}{4\sqrt{2}(NU_0\tilde{\Delta}_c\eta\chi)^{3/2}}. \tag{9}$$

In fact, the effective Hamiltonian (5) possesses a $\mathbb{Z}_2$ symmetry, as it is invariant under the simultaneous transformation of $\hat{a} \to -\hat{a}$ and $\hat{b}_j \to -\hat{b}_j$. The system spontaneously breaks this $\mathbb{Z}_2$ symmetry during the transition from the normal superfluid to superradiance [42].

III. RESULTS AND DISCUSSION

The key part of the phase condition (8) is the susceptibility χ of the normal phase, which characterizes the tendency of inducing superradiance. A larger χ indicates a greater critical magnitude of effective cavity detuning $|\tilde{\Delta}_c|$. Since we take the interference between two pumping lasers into account, the relation of χ to V_1 and V_2 cannot be separated independently, i.e., $\chi(V_1, V_2) \neq \chi_1(V_1)\chi_2(V_2)$, so it is infeasible to directly apply outcomes derived from the single-pump case for simplicity. We present numerical results for χ at zero temperature in Fig. 2 for different signs of atomic detuning Δ_a. In both cases, the susceptibility shows non-negativity $\chi \geqslant 0$. As expected, it is symmetric about $V_1 = V_2$, which renders it equivalent to fixing one of the pump depths while varying the other. However, in the case of $\Delta_a < 0$, χ grows as

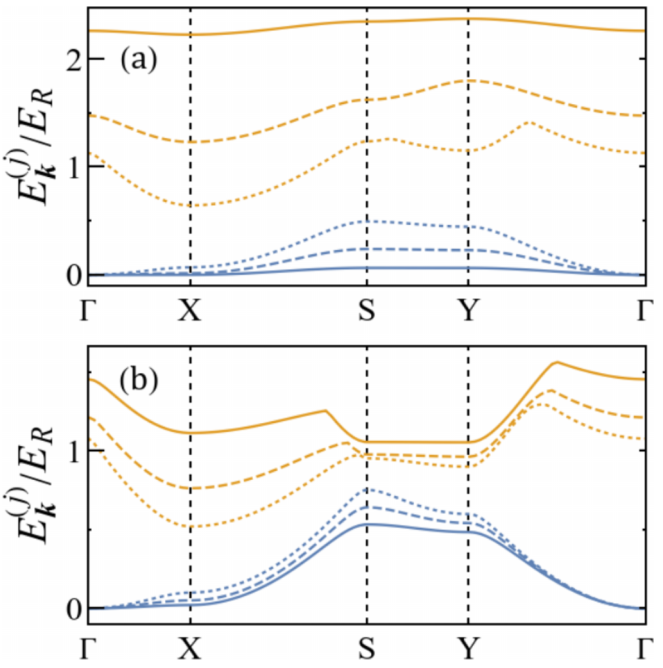

FIG. 3. Two lowest bands of the rectangular pump lattice for equal pump depths $V_1 = V_2$, with (a) $\Delta_a < 0$ and (b) $\Delta_a > 0$. Dotted, dashed, and solid lines are numerical results of pump lattice depths $0.5E_R$, E_R, and $2E_R$, respectively. Bands are calculated along points Γ, X, S, and Y marked in Fig. 1(b).

V_1 increases at given V_2, while for $\Delta_a > 0$ this monotonicity disappears as V_2 rises, and χ decreases to a local minimum towards $V_1 = V_2$. Furthermore, the growth rate of χ connected with $\Delta_a < 0$ is much larger than that with $\Delta_a > 0$. Within the range of $V_1, V_2 \in [0, 5E_R]$, the maximum $\chi_{\max}$ is over 4000 in Fig. 2(a), in comparison to $\chi_{\max} \sim 0.34$ in Fig. 2(b). This can be understood from the fact that the pump depths flatten the energy bands, as indicated in Fig. 3. Here we plot only the two lowest bands, which contribute the major parts of χ. Without loss of generality, pump depths are set to be equal so that pump potentials form a rectangular lattice, as shown in Fig. 1(c). It is clear that increasing the pump depths has a much more powerful effect on flattening energy bands and widening band gaps with negativity than positivity of Δ_a. Especially the first band width $E_1 - E_0$, which determines the denominator of the leading term in χ, becomes dominant at higher pump depths.

With susceptibility χ in hand, we are now in a position to construct phase diagrams. The pump lattice depths V_1 and V_2 can be tuned by varying the pump laser power, while the cavity detuning Δ_c can be controlled via cavity frequency ω_c. For experimental consideration, we construct phase diagrams in terms of experimentally tunable parameters V_1, V_2, and Δ_c.

A. Phase diagrams spanned by V_1 and Δ_c

Solving the phase boundary condition of Eq. (8) with respect to Δ_c yields the critical cavity detuning

$$\frac{\Delta_\pm}{NU_0} = \mathrm{sgn}(\Delta_a)\theta_c - 2\chi \pm \sqrt{4\chi^2 - \left(\frac{\kappa}{NU_0}\right)^2}, \tag{10}$$

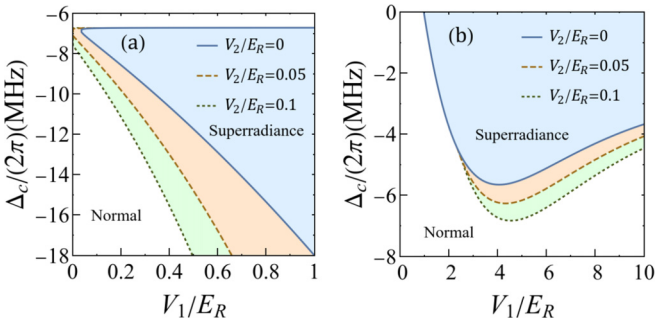

FIG. 4. Phase diagrams spanned by one of the pump lattice depths V_1/E_R and cavity detuning $\Delta_c/(2\pi$ MHz) for (a) $\Delta_a < 0$ and (b) $\Delta_a > 0$. Another pump depth is fixed at a small value $V_2/E_R < 1$. Experimental settings in Ref. [40] are used, with the atom number $N = 2.7 \times 10^5$, decay rate $\kappa = 2\pi \times 147$ kHz, atom-cavity coupling $g = 2\pi \times 1.95$ MHz, and magnitude of atomic detuning $|\Delta_a| = 2\pi \times 76.6$ GHz.

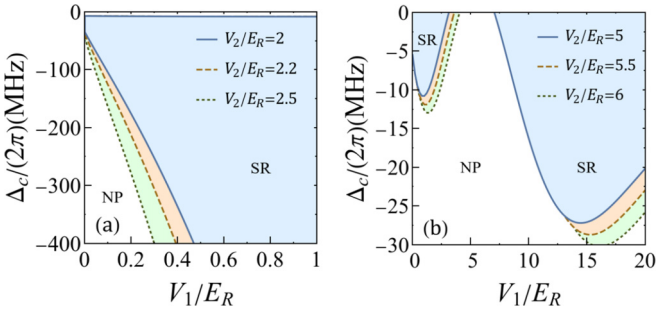

FIG. 5. Phase diagrams spanned by one of the pump lattice depths V_1/E_R and cavity detuning $\Delta_c/(2\pi$ MHz) for (a) $\Delta_a < 0$ and (b) $\Delta_a > 0$. Another pump depth is fixed at a comparable value $V_2/E_R > 1$. The other parameters are set to be the same as in Fig. 4. The acronym NP stands for the normal phase and SR for superradiance.

where we additionally define the scattering matrix element $\theta_c = \langle \Psi^{(1)}(0)| \cos^2(\mathbf{k}_c \cdot \mathbf{r})|\Psi^{(1)}(0)\rangle$ for convenience. It turns out that θ_c cannot be neglected when $\Delta_a > 0$, as θ_c is comparable to χ.

Here we consider only the situation that $\Delta_c < 0$. The reason is that, for $\Delta_c > 0$, the term $-\Delta_c \hat{a}^\dagger \hat{a}$ in Eq. (1) indicates that the system can lower its energy in the rotating frame with more photons and then gives rise to a transition from the metastable regime to the unstable regime [40]. In this situation, we have to care about large α and therefore the perturbation method breaks down. Instead, within $\Delta_c < 0$, we only need to deal with small α and the above results always hold. Hence, only negative solutions of Eq. (10) are taken into account. We map out the phase diagrams on V_1 and Δ_c at small V_2 in Fig. 4. Here we choose the parameters from Ref. [40] for verification, where the atom number $N = 2.7 \times 10^5$, the decay rate $\kappa = 2\pi \times 147$ kHz, the atom-cavity coupling $g = 2\pi \times 1.95$ MHz, and the magnitude of atomic detuning $|\Delta_a| = 2\pi \times 76.6$ GHz.

For $\Delta_a < 0$, both $\Delta_\pm$ are negative due to $\chi > 0$ and $\theta_c > 0$. At the limit $V_2 \to 0$, the phase boundary in Fig. 4(a) captures the characteristics of the well-known superradiant transition in the single-pump system: The cavity photons emerge and then vanish as the cavity detuning increases from below [12]. In addition, there is a threshold of V_1, here $V_1 \sim 0.03E_R$, below which the superradiance will not happen. The threshold can be obtained by requiring $\chi = \kappa/2NU_0$. However, this threshold will no longer exist while another pump depth V_2 rises, as exhibited by the boundaries of $0.05E_R$ and $0.1E_R$ in Fig. 4(a). In other words, if a system is in the superradiant phase with one pump laser, adding another pump will not drive it out. Further, increasing V_2 also makes the lower bounds of phase boundaries steeper and steeper, which indicates it is easier for the system to enter the superradiant phase.

However, situations are different in the case of $\Delta_a > 0$, where $\theta_c \sim 0.5$ is comparable to χ. That leaves only Δ_- being partially negative as a function of V_1 at the current parameter settings. At the limit $V_2 \to 0$, the phase boundary in Fig. 4(a) is in agreement with the numerical mean-field results in Ref. [40]. For a fixed cavity detuning Δ_c, such as $-2\pi \times 4$ MHz, the system starting in the normal phase undergoes a transition to the superradiant phase and returns to the normal phase as the pump lattice is ramped up. This uniqueness of the phase boundary is a result of the competition between the band gap and mode softening. Meanwhile, there is a local minimum of critical Δ_c for different V_2 and it gets lower as V_2 increases.

In the regime of a deeper pump lattice $V_2/E_R > 1$, the slope of the critical cavity detuning Δ_-, as a function of V_1, gets even steeper than in $V_2/E_R < 1$ for negative Δ_a, as shown in Fig. 5(a). This indicates an increasing tendency of a transition towards superradiance as the pump depth goes deeper, provided the pump lattice potentials are both attractive.

For positive Δ_a, another superradiant region shows up at higher pump depths $V_2/E_R > 1$. In this regime, the system enters the superradiant phase, returns to the normal phase, and then reenters the superradiant phase as the pump depth V_1 is ramped up, as illustrated in Fig. 5(b). In contrast to the case in $\Delta_a < 0$, if a system is in the superradiant phase with a single-pump laser, adding another pump will suppress superradiance within a certain range.

B. Phase diagrams spanned by V_1 and V_2

In the phase boundary condition of Eq. (8), not only χ, but also θ_c in $\tilde{\Delta}_c$ has a dependence on V_1 and V_2. It is useful to introduce the functions $f_\pm$ for $\mathrm{sgn}(\Delta_a) = \pm 1$, where

$$f_\pm = \chi + \frac{(\Delta_c/NU_0 \mp \theta_c)^2 + (\kappa/NU_0)^2}{4(\Delta_c/NU_0 \mp \theta_c)}. \tag{11}$$

Note that $f_\pm$ are dimensionless functions of V_1/E_R and V_2/E_R if Δ_c/NU_0 and κ/NU_0 are given. Here $\tilde{\Delta}_c < 0$ and $\Delta_c < 0$ restrict $\Delta_c/NU_0 < 0$ for $\Delta_a > 0$ and $\Delta_c/NU_0 < -\theta_c$ for $\Delta_a < 0$. Here $f_\pm > 0$ are the criteria for superradiance and $f_\pm < 0$ for the normal phase. In Fig. 6 we plot the phase diagrams for different cavity detunings Δ_c/NU_0 at the decay rate $\kappa/NU_0 = 0.1$.

Within $V_1, V_2 \leqslant 5E_R$, the area of the normal phase shrinks as Δ_c approaches 0 for both positive and negative Δ_a, in accordance with the above results. Now, if we keep the two pump depths equal $V_1 = V_2$ and increase them simultaneously, the system undergoes a transition from the normal phase to superradiance in the case of positive Δ_a, while for negative Δ_a the system remains in the normal phase. Notice that

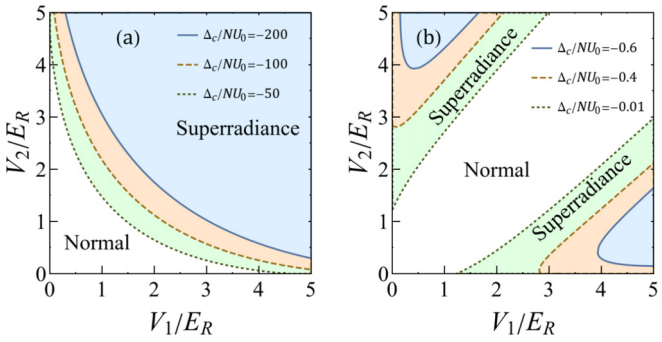

FIG. 6. Phase diagrams in terms of two pump lattice depths V_1/E_R and V_2/E_R with cavity detuning Δ_c/NU_0 fixed for (a) $\Delta_a < 0$ and (b) $\Delta_a > 0$. Here we set $\kappa/NU_0 = 0.1$.

there exists a diagonal region around $V_1 = V_2$ for the normal phase when $\Delta_a > 0$, even if Δ_c approaches zero, as shown in Fig. 6(b). Actually, one can derive that $f_+ < \chi - \theta_c/4$ is true for arbitrary $V_1, V_2 > 0$ in this case. Numerical results show that $\chi - \theta_c/4 \sim -0.1$, and thereby $f_+ < 0$, as two equal pump depths $V_1 = V_2 = V$ change within $10E_R$. In other words, if two pump depths are equal, the system will remain in the normal phase as the pump depth increases within a wide range (at least from 0 to $10E_R$), no matter how we choose κ and Δ_c. The same arguments apply to the neighborhoods of $V_1 = V_2$. From another point of view, if a system is in the superradiant phase with a single pump of depth V_1, adding another pump of V_2 will suppress superradiance for $V_2 \leqslant V_1$.

IV. CONCLUSION

We compared susceptibilities of a BEC inside two crossed pump fields for the red atomic detuning ($\Delta_a < 0$) and the blue atomic detuning ($\Delta_a > 0$). We mapped out phase boundaries separating the normal superfluid and the superradiance for the red cavity detuning ($\Delta_c < 0$). Phase diagrams were examined at the single-pump limit and they were also compared in the double-pump regime. We found that if a system is in the superradiant phase with one pump laser, adding another pump will keep the system in the superradiant phase when the atomic detuning is red ($\Delta_a < 0$), while for blue detuning ($\Delta_a > 0$), increasing another pump potential has a suppressive effect on the superradiance. Finally, we showed that equally increasing two pump potentials can also induce a transition from the normal phase to superradiance for red atomic detuning ($\Delta_a < 0$), while in the case of blue detuning ($\Delta_a > 0$) the system will remain in the normal phase as pump depths increase within a wide range, which is independent of the cavity detuning and decay rate. In this study, we focused on the case where the relative spatial phase ϕ between the pumps and the cavity field are zero. For nonzero ϕ, even the unperturbed Hamiltonian $\hat{\mathcal{H}}_0$ remains the same; the scattering operator $\hat{\Theta}$ now depends on ϕ, which renders the susceptibility χ dependent on ϕ as well. This can affect the density pattern in superradiance and the phase boundaries. How the phase boundaries and associated physical quantities vary with ϕ deserves further study. We believe that experimental verification of our predictions will contribute to a better understanding of superradiant transitions with ultracold gases in optical cavities.

ACKNOWLEDGMENTS

This work was supported by NSFC under Grants No. 12174055 and No. 11674058 and by the Natural Science Foundation of Fujian under Grant No. 2020J01195.

[1] H. Ritsch, P. Domokos, F. Brennecke, and T. Esslinger, Cold atoms in cavity-generated dynamical optical potentials, Rev. Mod. Phys. **85**, 553 (2013).
[2] V. D. Vaidya, Y. Guo, R. M. Kroeze, K. E. Ballantine, A. J. Kollár, J. Keeling, and B. L. Lev, Tunable-range, photon-mediated atomic interactions in multimode cavity QED, Phys. Rev. X **8**, 011002 (2018).
[3] F. Mivehvar, F. Piazza, T. Donner, and H. Ritsch, Cavity QED with quantum gases: New paradigms in many-body physics, Adv. Phys. **70**, 1 (2021).
[4] S. Ostermann, H. Ritsch, and F. Mivehvar, Many-body phases of a planar Bose-Einstein condensate with cavity-induced spin-orbit coupling, Phys. Rev. A **103**, 023302 (2021).
[5] P. Kongkhambut, J. Skulte, L. Mathey, J. G. Cosme, A. Hemmerich, and H. Keßler, Observation of a continuous time crystal, Science **377**, 670 (2022).
[6] D. Dreon, A. Baumgärtner, X. Li, S. Hertlein, T. Esslinger, and T. Donner, Self-oscillating pump in a topological dissipative atom–cavity system, Nature (London) **608**, 494 (2022).
[7] S. Ostermann, V. Walther, and S. F. Yelin, Superglass formation in an atomic BEC with competing long-range interactions, Phys. Rev. Res. **4**, 023074 (2022).
[8] L. Carl, R. Rosa-Medina, S. D. Huber, T. Esslinger, N. Dogra, and T. Dubcek, Phases, instabilities and excitations in a two-component lattice model with photon-mediated interactions, Phys. Rev. Res. **5**, L032003 (2023).
[9] J. Skulte, P. Kongkhambut, S. Rao, L. Mathey, H. Keßler, A. Hemmerich, and J. G. Cosme, Condensate formation in a dark state of a driven atom-cavity system, Phys. Rev. Lett. **130**, 163603 (2023).
[10] Y. Deng and S. Yi, Self-ordered supersolid phase beyond Dicke superradiance in a ring cavity, Phys. Rev. Res. **5**, 013002 (2023).
[11] N. Sauerwein, F. Orsi, P. Uhrich, S. Bandyopadhyay, F. Mattiotti, T. Cantat-Moltrecht, G. Pupillo, P. Hauke, and J.-P. Brantut, Engineering random spin models with atoms in a high-finesse cavity, Nat. Phys. **19**, 1128 (2023).
[12] K. Baumann, C. Guerlin, F. Brennecke, and T. Esslinger, Dicke quantum phase transition with a superfluid gas in an optical cavity, Nature (London) **464**, 1301 (2010).
[13] N. Defenu, T. Donner, T. Macrì, G. Pagano, S. Ruffo, and A. Trombettoni, Long-range interacting quantum systems, Rev. Mod. Phys. **95**, 035002 (2023).
[14] R. H. Dicke, Coherence in spontaneous radiation processes, Phys. Rev. **93**, 99 (1954).

[15] C. Maschler, I. B. Mekhov, and H. Ritsch, Ultracold atoms in optical lattices generated by quantized light fields, Eur. Phys. J. D **46**, 545 (2008).

[16] D. Nagy, G. Szirmai, and P. Domokos, Self-organization of a Bose-Einstein condensate in an optical cavity, Eur. Phys. J. D **48**, 127 (2008).

[17] D. Nagy, G. Kónya, G. Szirmai, and P. Domokos, Dicke-model phase transition in the quantum motion of a Bose-Einstein condensate in an optical cavity, Phys. Rev. Lett. **104**, 130401 (2010).

[18] K. Baumann, R. Mottl, F. Brennecke, and T. Esslinger, Exploring symmetry breaking at the Dicke quantum phase transition, Phys. Rev. Lett. **107**, 140402 (2011).

[19] K. J. Arnold, M. P. Baden, and M. D. Barrett, Self-organization threshold scaling for thermal atoms coupled to a cavity, Phys. Rev. Lett. **109**, 153002 (2012).

[20] F. Piazza, P. Strack, and W. Zwerger, Bose-Einstein condensation versus Dicke-Hepp-Lieb transition in an optical cavity, Ann. Phys. (NY) **339**, 135 (2013).

[21] J. Klinder, H. Keßler, M. Wolke, L. Mathey, and A. Hemmerich, Dynamical phase transition in the open Dicke model, Proc. Natl. Acad. Sci. USA **112**, 3290 (2015).

[22] Z. Zhiqiang, C. H. Lee, R. Kumar, K. J. Arnold, S. J. Masson, A. S. Parkins, and M. D. Barrett, Nonequilibrium phase transition in a spin-1 Dicke model, Optica **4**, 424 (2017).

[23] M. Landini, N. Dogra, K. Kroeger, L. Hruby, T. Donner, and T. Esslinger, Formation of a spin texture in a quantum gas coupled to a cavity, Phys. Rev. Lett. **120**, 223602 (2018).

[24] R. M. Kroeze, Y. Guo, V. D. Vaidya, J. Keeling, and B. L. Lev, Spinor self-ordering of a quantum gas in a cavity, Phys. Rev. Lett. **121**, 163601 (2018).

[25] Z. Zhang, C. H. Lee, R. Kumar, K. J. Arnold, S. J. Masson, A. L. Grimsmo, A. S. Parkins, and M. D. Barrett, Dicke-model simulation via cavity-assisted Raman transitions, Phys. Rev. A **97**, 043858 (2018).

[26] A. Morales, D. Dreon, X. Li, A. Baumgärtner, P. Zupancic, T. Donner, and T. Esslinger, Two-mode Dicke model from nondegenerate polarization modes, Phys. Rev. A **100**, 013816 (2019).

[27] X. Li, D. Dreon, P. Zupancic, A. Baumgärtner, A. Morales, W. Zheng, N. R. Cooper, T. Donner, and T. Esslinger, First order phase transition between two centro-symmetric superradiant crystals, Phys. Rev. Res. **3**, L012024 (2021).

[28] S. Sachdev, *Quantum Phase Transitions*, 2nd ed. (Cambridge University Press, Cambridge, 2011).

[29] E. Fradkin, S. A. Kivelson, and J. M. Tranquada, *Colloquium*: Theory of intertwined orders in high temperature superconductors, Rev. Mod. Phys. **87**, 457 (2015).

[30] A. Morales, P. Zupancic, J. Léonard, T. Esslinger, and T. Donner, Coupling two order parameters in a quantum gas, Nat. Mater. **17**, 686 (2018).

[31] J. Léonard, A. Morales, P. Zupancic, T. Esslinger, and T. Donner, Supersolid formation in a quantum gas breaking a continuous translational symmetry, Nature (London) **543**, 87 (2017).

[32] J. Lang, F. Piazza, and W. Zwerger, Collective excitations and supersolid behavior of bosonic atoms inside two crossed optical cavities, New J. Phys. **19**, 123027 (2017).

[33] Z. Wu, Y. Chen, and H. Zhai, Emergent symmetry at superradiance transition of a Bose condensate in two crossed beam cavities, Sci. Bull. **63**, 542 (2018).

[34] R. R. Soldati, M. T. Mitchison, and G. T. Landi, Multipartite quantum correlations in a two-mode Dicke model, Phys. Rev. A **104**, 052423 (2021).

[35] J. Léonard, A. Morales, P. Zupancic, T. Donner, and T. Esslinger, Monitoring and manipulating Higgs and Goldstone modes in a supersolid quantum gas, Science **358**, 1415 (2017).

[36] J. Keeling, M. J. Bhaseen, and B. D. Simons, Collective dynamics of Bose-Einstein condensates in optical Cavities, Phys. Rev. Lett. **105**, 043001 (2010).

[37] N. Liu, J. Lian, J. Ma, L. Xiao, G. Chen, J. Q. Liang, and S. Jia, Light-shift-induced quantum phase transitions of a Bose-Einstein condensate in an optical cavity, Phys. Rev. A **83**, 033601 (2011).

[38] M. J. Bhaseen, J. Mayoh, B. D. Simons, and J. Keeling, Dynamics of nonequilibrium Dicke models, Phys. Rev. A **85**, 013817 (2012).

[39] F. Mivehvar, H. Ritsch, and F. Piazza, Superradiant topological Peierls insulator inside an optical cavity, Phys. Rev. Lett. **118**, 073602 (2017).

[40] P. Zupancic, D. Dreon, X. Li, A. Baumgärtner, A. Morales, W. Zheng, N. R. Cooper, T. Esslinger, and T. Donner, *P*-band induced self-organization and dynamics with repulsively driven ultracold atoms in an optical cavity, Phys. Rev. Lett. **123**, 233601 (2019).

[41] Y. Chen, Z. Yu, and H. Zhai, Superradiance of degenerate Fermi gases in a cavity, Phys. Rev. Lett. **112**, 143004 (2014).

[42] J. Léonard, A supersolid of matter and light, Ph.D. thesis, ETH Zurich, 2017, https://doi.org/10.3929/ethz-b-000262194.